sustainability

Article

Research on Design and Optimization of Large Metal Bipolar Plate Sealing for Proton Exchange Membrane Fuel Cells

Jinghui Zhao [1,2,3], Huijin Guo [1,2,3], Shaobo Ping [3,4], Zimeng Guo [3], Weikang Lin [1,2], Yanbo Yang [1,2], Wen Shi [3], Zixi Wang [5] and Tiancai Ma [1,2,*]

1 School of Automotive Studies, Tongji University, No. 4800 Caoan Highway, Shanghai 201804, China; zhaojinghui@tongji.edu.cn (J.Z.); 1811472@tongji.edu.cn (H.G.); weikang.lin@tongji.edu.cn (W.L.); yanboyang@tongji.edu.cn (Y.Y.)
2 Institute of Carbon Neutrality, Tongji University, Shanghai 200092, China
3 AT&M Environmental Engineering Technology Co., Ltd., No. 76 Xueyuan South Road, Haidian District, Beijing 100081, China; pingshaobo@atmcn.com (S.P.); guozimeng@atmcn.com (Z.G.); schumy_shi@aliyun.com (W.S.)
4 Technology Innovation Center, Central Iron and Steel Research Institute Group, Beijing 100081, China
5 Department of Mechanical Engineering, Tsinghua University, Beijing 100084, China; zxwang@tsinghua.edu.cn
* Correspondence: matiancai@tongji.edu.cn

Abstract: The sealing system, as the most important load-bearing component, is a critical part of the stack assembly in a proton exchange membrane fuel cell (PEMFC). Currently, flat or single-peak sealing gaskets are commonly used for large metal bipolar plate sealing, which can easily cause problems such as significant internal stress and distortion displacement. In order to solve this problem, an innovative double-peak sealing gasket structure is proposed. Based on the Mooney–Rivlin constitutive model, the impact of the sealing material hardness, friction coefficient, and compression ratio on the sealing performance are investigated. Meanwhile, the double-peak seal is fabricated and assembled into a single fuel cell for testing. The results show that the sealing performance of a double-peak sealing gasket with extended wings has been optimized, and the maximum contact pressure on the upper and lower contact surfaces is 1.2 MPa and 0.67 MPa, respectively, which is greater than the given air pressure of 0.1 MPa. And the sealing effect is optimal with a 45 Shore A hardness rubber, a friction coefficient of 0.05, and an initial compression ratio of 35%. The simulation and experimental sealing performance of the sealing gasket under different compression ratios remain similar.

Keywords: PEMFC; metal bipolar plate; double-peak sealing gasket; sealing design and optimization; compression ratio

Citation: Zhao, J.; Guo, H.; Ping, S.; Guo, Z.; Lin, W.; Yang, Y.; Shi, W.; Wang, Z.; Ma, T. Research on Design and Optimization of Large Metal Bipolar Plate Sealing for Proton Exchange Membrane Fuel Cells. *Sustainability* **2023**, *15*, 12002. https://doi.org/10.3390/su151512002

Academic Editors: Laisuo Su, Jun Huang, Shikhar Jha, Biyu Jin and Yubai Li

Received: 15 June 2023
Revised: 24 July 2023
Accepted: 2 August 2023
Published: 4 August 2023

1. Introduction

Among the many renewable energy sources, hydrogen energy represents the new energy paradigm. It has obtained much attention from research institutes and industrial companies in many countries due to its high energy density, environmentally friendly process, non-pollutant emissions (only water is produced as the reaction product), and relatively abundant source [1–4]. Due to their few moving parts, low operating temperature, high efficiency, and environmentally friendly adaptability, proton exchange membrane fuel cells (PEMFCs), which use hydrogen as fuel, have become the most promising application technology in fuel cell vehicles [5,6].

Typically, a fuel cell stack consists of hundreds of individual cells connected in series, each composed of a seal, a bipolar plate, and a membrane electrode assembly (MEA). The seals are essential components for the gas tightness and stability of the PEMFC stack, which are applied to keep the reactant gases and coolant within their respective regions in the metal bipolar plate and the MEA. Based on the sealing method, the seals in fuel cells can generally be divided into two categories: the solid gasket and the liquid sealant [7]. The solid gasket is typically made of silicon rubber or fluorine rubber, such as silicone rubber, fluoroelastomer, and ethylene propylene diene monomer (EPDM), through molding or stamping while the liquid sealant is applied to the sealing surface before it is been cured. Currently, solid gaskets are often used in fuel cell stacks, which are suitable for exposure to hydrogen, humidified air, and acidic environments, and can also withstand mechanical stress and high temperatures [8–10]. And they need to meet specific requirements to prevent reactant gas leakage at a certain pressure in the PEMFC environment.

The chemical and mechanical properties of the seals determine the compression state and sealing ability [11]. And the long-term stability and durability of the seals have always been the key topics affecting the sealing performance of PEMFCs. Thus, more researchers have paid more attention to the chemical and mechanical degradation of the seal materials, the sealing structures, and the deformation of the PEMFC stack assembly. Wang et al. [12] studied the mechanical degradation of silicone rubber gaskets in PEMFCs under the conditions of two compressive loads and two simulated environments. The results found that adding silica to silicone rubber can significantly improve the stress relaxation performance of silicone rubber. Tan [13–15], Schulze [16], Lin [17], and Mitra [18,19] analyzed the chemical degradation of different rubber materials exposed to high-concentration solutions when simulating and accelerating the PEMFC environment. The loss of the seal materials caused by chemical degradation could lead to seal failure. Feng et al. [20] investigated the degradation of silicone rubbers with different hardnesses in various aqueous solutions. They found that silicone rubbers became more durable in aqueous solutions with the increase in hardness. Cui et al. [21,22] reported the sealing force and thermal stress development of silicone rubbers under temperature cycling. They found that thermal expansion or contraction are the major factors affecting the contact pressure, and pointed out that increases in the elasticity modulus are mainly caused by thermal expansion. Chien et al. [23] introduced the sealing system of PEMFCs and studied the compression of the seal by experimentation. By immediate in situ measurement of the thickness of the seal or the gap spacing after assembly and during a thermal cycle of the PEMFC, the variation of the compressive strain applied to the seal is characterized as the temperature of the PEMFC changes and cycles, thus estimating the sealing force in the stack and, consequently, the life prediction of the seal. Zhang et al. [24] investigated the stress–strain distribution of the fuel cell sealing structure at different operating temperatures and the effects of the compression ratio, fluid pressure, dislocations, and gasket size on the sealing performance and mechanical behavior of PEMFC. The results show that the surface temperature has a great influence on the equivalent stress of the sealing system and the deformation of the MEA frame. With the increase in the compression ratio and the size of the sealing ring, the deformation of the rubber ring is aggravated, the equivalent stress is increased, and the sealing performance is better. Achenbach [25,26] used numerical simulations to study the effect of stress relaxation and degradation on the lives of seals under different environments. They presented a service life prediction technique based on the principle of chemical deterioration rates and the strain energy density concept, and were able to approximately predict the service life of elastic seals. Su et al. [27] established a numerical model that relates assembly load with the porosity and permeability of the gas diffusion layer (GDL) for the purpose of evaluating the sealing performance of the stack, and also concluded that an optimal stacking load exists. The importance of the proper use of transport properties for the compressed portion of the GDL was found. Xing et al. [28] combined finite element analysis with experimental results to establish a relationship between the clamping torque during the stack assembly process and the compression level of the sealing gasket ring in the stack. The results showed that the relationship between the GDL compression, gasket, and sealing groove was quantitatively introduced to explain how the geometric parameters of the gasket affect the cell performance. And it was concluded that the applied torque, GDL compression, gasket, and sealing groove should be reasonably matched to reduce the ohmic resistance and avoid mass transfer limitation.

Although there is substantial literature discussing the effects of sealing material characteristics by themselves in PEMFC, the sealing structure design is also related to the sealing performance of PEMFC, which is key. The metal rubber composite sealing structure in the fuel cell metal stack is achieved by stamping the metal bipolar plate into a convex structure of an arch or trapezoid shape, and then setting a seal on the convex structure to enhance the performance of the sealing contact surface. Currently, the cross-section profiles of the seals used in fuel cell metal bipolar plates are typically flat or with a single-peak. That is, the cross-sectional shape of the sealing line on either side of the membrane electrode is rectangular or close to circular (or elliptical).

In the stack assembly process with multiple plates, the sealing section with a flat rectangular sealing structure, which formed a large contact surface, could enhance the stability of the stack. However, it is more sensitive to the sealing pressure on a larger contact surface, and greater compression strain may cause excessive internal stress and consequent failure. The single-peak sealing structure is prone to misalignment of the sealing gasket, causing shifts of the seal and shear stress and distortion of the plates between the contact points. Opposite pressure on the contact positions between the membrane electrode frame, the bipolar plate on both sides, and the sealing gasket results in reduced structural stability of the membrane electrode and bipolar plate, which affects the durability of the sealing and the service life of the fuel cell stack. Consequently, the single-peak sealing structure reduces the structural stability of the MEA components and the bipolar plates, leading to leakage and sealing failure of the PEMFC, thus affecting the durability of fuel cell stacks.

Currently, the problems of sealing leakage and deformation caused by the single-peak sealing structure are becoming increasingly prominent in practical engineering applications. This paper mainly proposes an innovative double-peak sealing gasket structure to solve the problems of sealing leakage and deformation while exploring the effects of rubber material properties, friction coefficient, and compression ratio on the airtightness of the seals and metal bipolar plates. The objective of this paper was to find matching sealing material characteristics and process parameters to guide the selection of the sealing materials and the stack assembly design of PEMFCs.

2. Sealing Principle and Sealing Structure

2.1. Principle of Elastomer Seal for Metal Plates

The bipolar plates, membrane electrode assembly (MEA), and sealing gasket form a gas-sealed chamber in the fuel cell metal stack. The seal forms two contact surfaces with the MEA and bipolar plate, respectively. Under the working pressure of the reactant gas, the sealing gasket tends to move outwards. This is balanced by the friction force at the compressed contact surfaces under compression. Under the assembly load of the cell stack, the sealing gasket undergoes compression deformation, producing a sealing force that resists gas leakage at the contact surface.

To ensure sealing performance, three factors need to be considered. First, the bipolar plate must have a feature to limit the gasket position. The rubber gasket is prone to deformation under compression. Without a design to constrain the gasket displacement, achieving an effective seal by accurately fitting the gasket to the sealing surface during assembly is challenging. Therefore, the metal bipolar plate normally has a sealing groove to fit the sealing gasket. Second, the sealing gasket must reach the required compression ratio under a certain assembly load to resist gas pressure and ensure the stability of the sealing structure. Third, at the micro level, leakage in the static sealing structure is mainly caused by the leak paths formed due to the roughness of the sealing interface [29]. The main function of the metal bipolar plate seal is to seal the gas using the deformed rubber under the fuel cell operating conditions. A preliminary model of the metal bipolar plate and composite rubber seal can be created based on the principle of interface leakage.

2.2. Sealing Structure Design

The schematic diagram of the sealing area on the large-sized bipolar plate is shown in Figure 1. The plate substrate was made of 316 L stainless steel with a thickness of 0.1 mm, and the overall size of the bipolar plate was 396 mm × 156 mm × 1 mm. The yellow and orange areas represent the sealing grooves, with a depth of 0.4 mm. Two different cases were studied to understand the impact of seal alignment during assembly: (1) the yellow well-aligned sealing grooves scenario (cross-section shown in Figure 1a), where the sealing grooves of the anode plate and cathode plate aligned well with each other; (2) the orange misaligned sealing groove scenario (cross-section shown in Figure 1b), where the sealing grooves of the anode plate and cathode plate had an offset from each other, mainly located at the gas–liquid inlet and outlet of the metal bipolar plate.

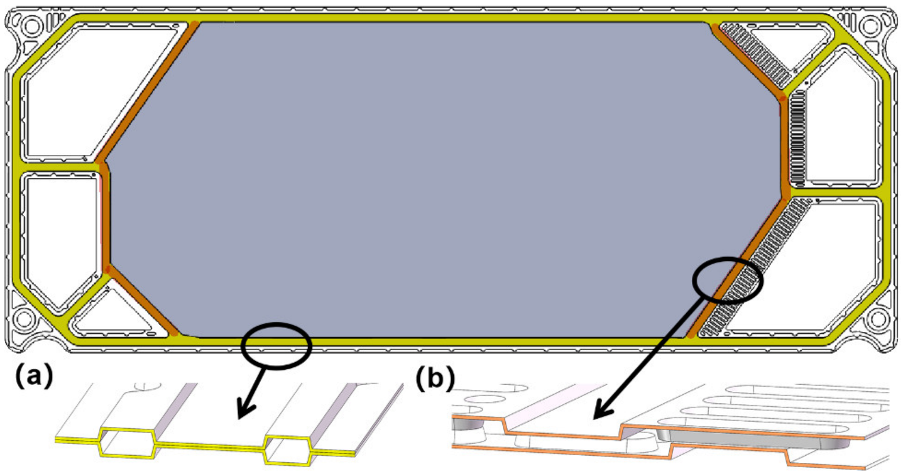

Figure 1. Geometric model of the metal bipolar plate. (**a**) Aligned sealing groove structure, (**b**) misaligned sealing groove structure.

Three typical PEMFC sealing materials are silicone rubber, fluoro rubber, and polyolefin rubber. Their aging mechanisms and stress relaxation properties are the focus of current research [7,14–17,30–33]. Silicone rubber is the most studied PEMFC-sealing material. It has lower chemical corrosion resistance and the worst durability performance among the three sealing materials [15,16]. Fluoro rubber is inferior to silicone rubber and polyolefin rubber in terms of low-temperature resistance, and its application is limited due to its complex production process and relatively high cost [14,33]. Therefore, polyolefin rubber is currently the best overall performance PEMFC-sealing material, mainly including EPDM and polyisobutylene rubber [17,34,35]. EPDM has good acid resistance, higher crosslink density, higher hardness, and a greater sealing force, and it is extensively studied in polyolefin rubber materials. EPDM was selected as the simulation and test material for this study.

Compared with single-peak and single-double-peak structures, the double-peak sealing structure has the lowest leakage rate and the highest sealing stability. In this paper, structural designs with different sealing gasket shapes and combinations were analyzed, as shown in Figure 2a–d. The uppermost and lowermost structures in the figure represent the metal bipolar plate, and the dark gray structures in contact with the metal bipolar plate represent the upper and lower sealing gaskets. The structure between the two sealing gaskets is the membrane electrode frame. Figure 2a–c were applied to the metal bipolar plate with a facing sealing groove structure. The structure of Figure 2a was modified from a single-peak sealing gasket to a double-peak sealing gasket to increase the sealing contact area. Figure 2b considers that the structure of the double peak facing the membrane electrode frame made it difficult to align the sealing gaskets of the cathode and anode electrodes during the actual paving process; thus, the double peaks of the cathode and anode sealing gasket were in contact with the bipolar plate, as is the structure of Figure 2c. Figure 2d was applied to the metal bipolar plate with a staggered sealing groove structure, where the sealing area was the gas–liquid inlet and outlet area. The airflow changed violently, the periodic characteristics were significant, and the air pressure was high. The sealing gasket usually tended to be misaligned. Therefore, we considered offsetting the sealing structure to adapt to this change, as shown in Figure 2d. The two wings of the sealing gasket were extended and staggered to fit the metal bipolar plate and to achieve sealing effects in the up and down relative positions.

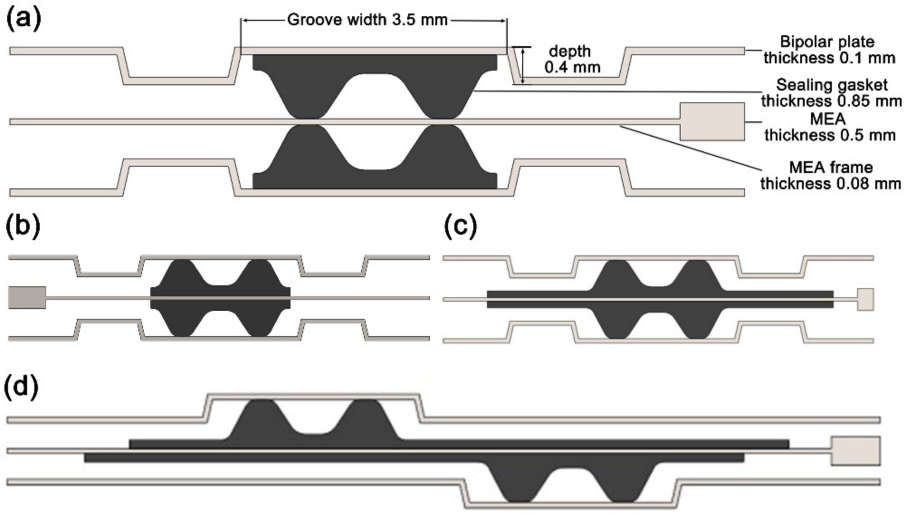

Figure 2. Schematic diagram of the seal structure design models. (**a**) Seal structure NO. 1, (**b**) seal structure NO. 2, (**c**) seal structure NO. 3, (**d**) the offset seal structure.

As shown in Figure 2a above, the thickness of the metal electrode plate was 0.1 mm, the thickness of the membrane electrode was 0.5 mm, the thickness of the membrane electrode frame was 0.08 mm, and the thickness of the seal gasket was 0.85 mm. The sealing gasket with an edge had an edge thickness of 0.15 mm, and the width and depth of the seal groove were 3.5 mm and 0.4 mm, respectively. The model's overall size was 10 mm × 10 mm × 1.98 mm.

3. Experimental and Simulation Theory

3.1. Finite Element Model and Sealing Requirements

Due to the unique nature of the sealing rubber material, the following assumptions can be made for the physical model of this paper [24]:

1. The rubber material has a general elastic modulus E and Poisson's ratio μ.
2. Although rubber materials have Poisson's ratio, their actual Poisson's ratio is 0.5, which is an incompressible material. In this paper, it is assumed that its Poisson's ratio is 0.49.
3. The creep properties of the sealing gasket are the same in all directions. The volume of the sealing gasket is not affected by material creep.
4. The stiffness of the groove made of steel components is several times that of rubber and can be considered as the constrained boundary when the gasket deforms.

The material property parameters of the metal bipolar plate and the membrane electrode frame in the simulation model are shown in Table 1:

Table 1. The material property parameters of the metal bipolar plate and the MEA frame in the simulation model.

Component	Young's Modulus/MPa	Poisson's Ratio
Metal bipolar plate	193,000	0.27
MEA frame	17,640	0.3

The Mooney Rivlin model is generally used to simulate the mechanical behavior of rubber materials under small and medium deformation conditions, and different parameter models are used for different deformation ranges. Since the gasket material in this study is EPDM rubber, and the compression ratio is less than 40%, the Mooney–Rivlin model with two parameters was considered, and the strain energy function corresponding to the two parameters was as shown in Equation (1) [26]:

$$W = C_{10}(I_1 - 3) + C_{01}(I_2 - 3) \tag{1}$$

where W is the density of the strain energy; C_{10} and C_{01} are the material coefficients of the gasket in the Mooney–Rivlin model, and I_1 and I_2 are the invariants of the first and second strain tensors.

The formula of stress σ' and strain ε is as shown in Equation (2):

$$\sigma' = \partial W / \partial \varepsilon \tag{2}$$

The values of parameters C_{10} and C_{01} under different hardnesses are shown in the Table 2:

Table 2. The values of parameters C_{10} and C_{01} under different hardnesses.

Hardness (Shore A)	C_{10}/MPa	C_{01}/MPa
45	0.2341	0.0513
50	0.2897	0.0599
55	0.3744	0.0657
60	0.4947	0.0639

The rubber hardness range studied in this article was 45 Shore A, 50 Shore A, 55 Shore A, and 60 Shore A, with friction coefficients covering 0.05, 0.1, 0.15, and 0.2, and compression ratios including 25%, 30%, 35%, and 40%.

In this article, the compression ratio δ is defined by the variation in the cross-sectional height of the sealing gasket, as shown in Equation (3):

$$\delta = (d_1/d_2) \cdot 100\% \tag{3}$$

In the formula, δ represents the compression ratio of the sealing gasket, d_1 represents the distance to which the sealing gasket is compressed in the direction of its cross-sectional height, and d_2 represents the initial height of the sealing gasket's cross-sectional plane.

Generally speaking, the design criteria for gaskets are as follows:

Failure criteria: In order to ensure that the sealing structure does not fail, a minimum contact stress criterion must be met. That is, according to the sealing theory, the sufficient and necessary condition for achieving reliable sealing is that the contact stress on the continuous interface between the gasket and the groove surface is not less than the given gas pressure, as shown in Equation (4).

$$(\sigma)_{max} \geq P \tag{4}$$

where σ is the contact stress on the continuous interface between the gasket and the groove surface, and P is the gas pressure at the air inlet of the metal bipolar plate.

Considering the actual working conditions of the fuel cell metal bipolar plate sealing, due to the uneven distribution of contact pressure between the MEA, bipolar plate, and sealing gasket, it is not accurate enough to judge the sealing performance by the maximum contact stress in Equation (4) alone.

Figure 3 is a schematic diagram of the sealing gasket under the action of encapsulation force and air working pressure. According to mechanical principles, if the working pressure of the air inside in the fuel cell is P, the sealing gasket must form an effective sealing surface after compression. The sealing conditions that should be met are:

$$\mu\sigma S_2 \geq PS_1 \quad (5)$$

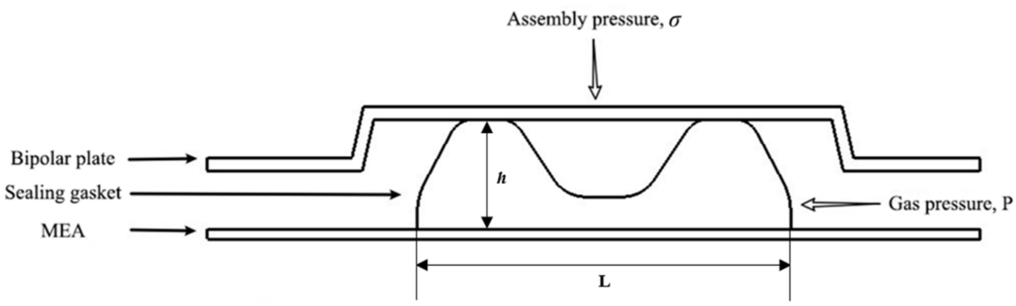

Figure 3. Schematic diagram of sealing gasket under encapsulation force and air working pressure.

Considering that the axial length of the sealing gasket is fixed during numerical simulation, the sealing areas S_1 and S_2 are replaced by straight lines h and L. Equation (5) becomes:

$$\mu\sigma L \geq Ph \quad (6)$$

where μ is the coefficient of friction, σ is the contact pressure of the upper or lower contact surface of the sealing gasket, S_1 is the contact area between the sealing gasket and the working gas after compression, S_2 is the contact area between the sealant and the bipolar plate after compression, L is the length of the contact surface along the width direction of the sealing gasket, P is the pressure at the air inlet of the metal bipolar plate, and h is the height of the compressed sealing gasket.

Therefore, Equation (7) below can be used to characterize the force on the sealing gasket by the average contact pressure, thus meeting the gas' sealing requirements.

$$\mu\overline{\sigma} L \geq Ph \quad (7)$$

where $\overline{\sigma}$ is the average contact pressure of the upper or lower contact surface of the sealing gasket.

Based on the design concept in Figure 2, a three-dimensional model of the sealing structure was established for finite element analysis, as detailed in Section 4.

The simulation uses ANSYS2021 static structural analysis module. The contact problem belongs to the functional extremum problem with constraints, and the penalty function method was used. The friction model was the Coulomb friction model. The computing hardware resources were 64-bit 4-core workstations, including 32 G RAM, Windows 10 system, and 3.6 GB CPU. During the simulation, the lower metal plate was fixed. A compression load was applied to the upper metal electrode plate to compress the sealing gasket. Frictional contact existed between the sealing gasket and the metal electrode plate, as well as between the sealing gasket and the membrane electrode frame. The friction coefficient under water lubrication conditions was 0.05. Since the elastic modulus of the metal plate was much larger than that of the sealing gasket, deformation mainly occurred in the sealing gasket. The thickness of the sealing gasket was 0.85 mm, and the model had two layers with a total thickness of 1.7 mm. To simulate the compression ratio of 30%, the displacement load needed to be set to 0.51 mm.

3.2. Sealing Performance Experiment

The sealing performance was measured by the pressure drop method, as shown in Figure 4. During detection, air entered through the inlet, passed through the shut-off valve 1 and the pressure gauge 2, and entered test device 3. In the experiment, the airflow rate was adjusted, and when the pressure gauge reached 0.1 MPa, the shut-off valve was closed, and the change in the pressure gauge reading measured the leakage of the test container.

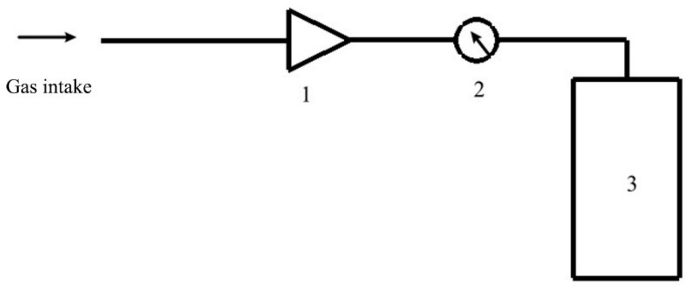

Figure 4. Schematic diagram of the pressure-drop method's leak detection principle.

The material of the metal bipolar plate was 316 L. Membrane electrode assembly from TangFeng Energy (Shanghai, China) was used for the test, with a thickness of 0.5 mm and a compression ratio of 20% to 30%. The frame thickness of the membrane electrode was 0.08 mm. The sealing groove and gasket at the non-gas-liquid inlet and outlet of the metal bipolar plate used the sealing structure shown in Figure 2c, while the sealing groove and gasket at the gas–liquid inlet and outlet used the staggered sealing structure shown in Figure 2d. The gasket material was a 45 Shore A hardness EPDM rubber with a surface roughness of 0.08 mm. Figure 5 shows the installation effect of the gasket on the metal bipolar plate, where Figure 5a shows the gasket bonded to the metal bipolar plate, and Figure 5b shows the gasket connected to the membrane electrode. And a physical cross-sectional view of the double-peaked gasket with extended wings is shown. The two metal bipolar plates, one membrane electrode, four gaskets, and front and rear plates were assembled into a single fuel cell for the sealing test.

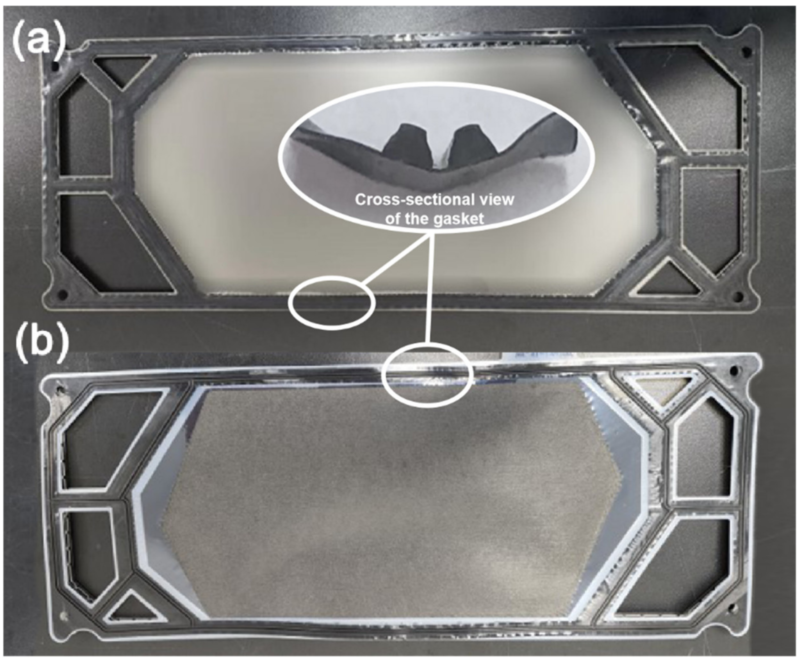

Figure 5. Installation effect of the gasket on the metal bipolar plate. (**a**) Gasket bonded to the bipolar plate. (**b**) Gasket bonded to the MEA.

In addition, the assembled single fuel cell was placed on the press, the leak detection device was connected, and the sealing performance test was conducted by adjusting the compression ratio of the tested single fuel cell through microcomputer control of the press. The average compression ratios of the gaskets were controlled at 25%, 30%, 35%, and 40%, respectively, and the pressure gauge readings were recorded for 10 min.

3.3. The Path-Flow Procedures of the Research

Compared with flat or single-peak structures, a double-peak sealing structure can enhance the performance by effectively mitigating the risk of high internal stress with a flat seal and misalignment with a single-peak seal. A double-peak sealing structure was studied in this work. Different combinations of the double-peak sealing structure gaskets and metal bipolar plates were designed. Based on the established geometric model and the Mooney–Rivlin constitutive model, numerical simulation and analysis were carried out by using ANSYS. The impacts of the sealing material hardness, friction coefficient, and compression ratio on the sealing performance were also investigated. Meanwhile, the double-peak seal was fabricated and assembled into a single fuel cell for testing. The path-flow procedures of the research on the double-peak sealing structure are shown in Figure 6.

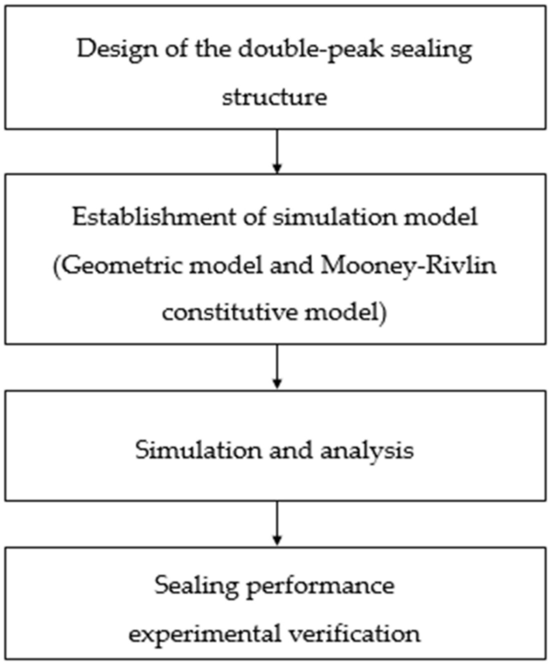

Figure 6. The path-flow procedures of the research on the double-peak sealing structure.

4. Results and Discussion

4.1. Simulation Analysis of Different Sealing Structures

Figure 7 shows the pressure distribution on the sealing contact surface after simulating and analyzing the seal structure NO. 1 gasket in Figure 2a.

Considering that the double-peak structure of the upper and lower gaskets in Figure 2a is challenging to align completely in actual engineering operations, the upper gasket was shifted 0.05 mm to the left to simulate real working conditions, and the simulation results are shown in Figure 8. Compared with the non-shifted case, the difference in contact pressure after shifting was insignificant. The maximum pressure on the upper contact surface was 0.72 MPa and that on the lower contact surface was 1.28 MPa after shifting, whereas the maximum pressure on the upper contact surface was 0.69 MPa and that on the lower contact surface was 1.37 MPa before shifting. However, the pressure distribution after shifting was not uniform and symmetrical enough, which can cause deformation of the MEA frame and increase the risk of leakage.

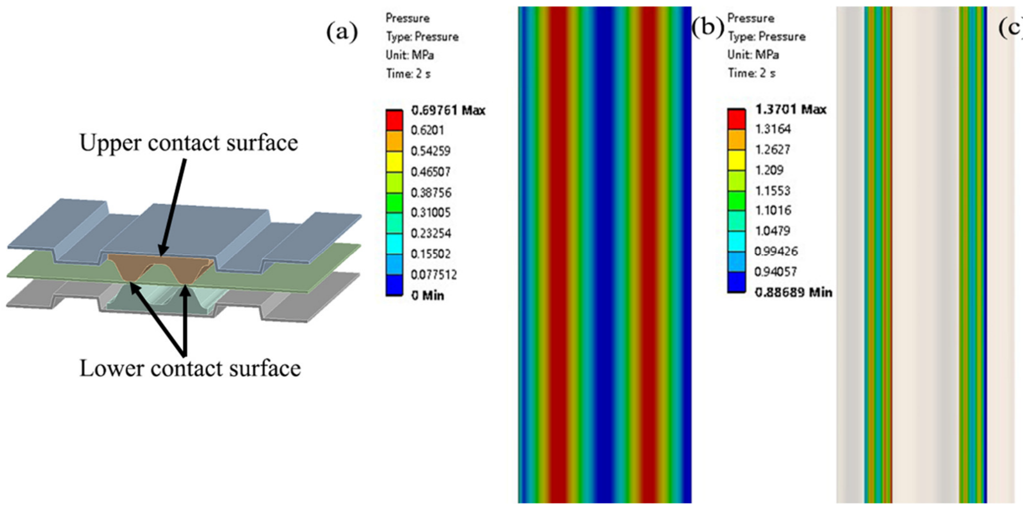

Figure 7. Pressure distribution on the contact surface of the seal structure NO. 1 gasket. (**a**) Sealing structure, (**b**) upper contact surface, (**c**) lower contact surface.

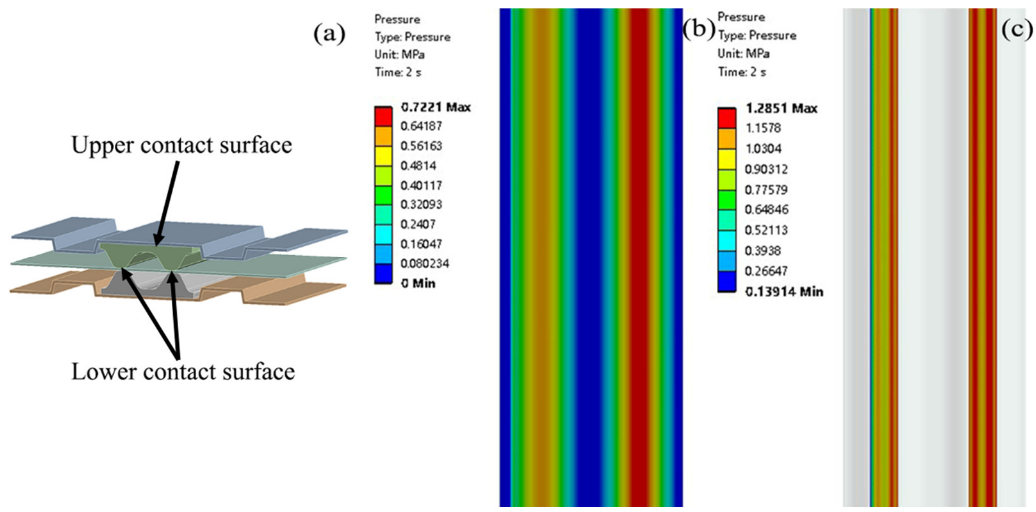

Figure 8. Pressure distribution on the contact surface of the seal structure NO. 1 gasket with the upper gasket was shifted 0.05 mm to the left. (**a**) Sealing structure, (**b**) upper contact surface, (**c**) lower contact surface.

Compared with the sealing structure NO. 1 shown in Figure 2a, the seal structure NO. 2 in Figure 2b adjusted the placement order of the double-peak sealing gasket, with the two peaks of the upper and lower sealing gaskets attached, respectively, to the bipolar plate to reduce the error caused by the misalignment of the two peaks during operation and to improve the sealing performance. Figure 9 shows the pressure distribution on the upper and lower contact surfaces after simulation and analysis using the sealing structure shown in Figure 2b. The simulation results show that the maximum pressure on the upper contact surface of the sealing gasket was 1.36 MPa, and the maximum pressure on the lower contact surface was 0.69 MPa.

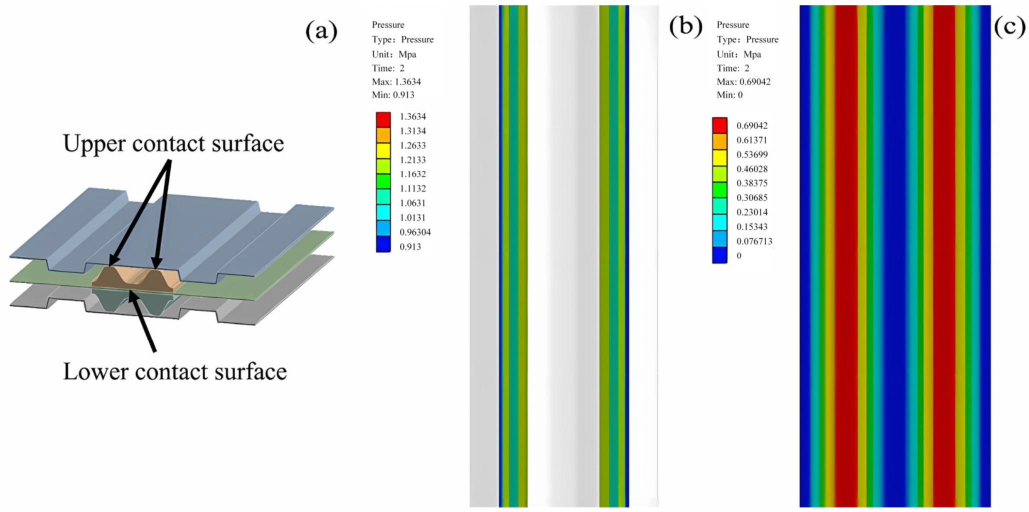

Figure 9. Pressure distribution on the contact surface of the seal structure NO. 2 gasket. (**a**) Sealing structure, (**b**) upper contact surface, (**c**) lower contact surface.

Compared with the sealing structures NO. 1 and NO. 2 in Figure 2a,b, the seal structure NO. 3 in Figure 2c has a design of outward extension on the two wings of the double-peak sealing gasket to enhance the sealing effect. Figure 10 shows the equivalent stress distribution of the double-peak sealing gasket with the outward extension on the two wings, indicating that this new structure's maximum equal stress was 0.64 MPa, far less than the allowable stress of the material, which is 6 MPa. Figure 11 shows the pressure distribution on the upper and lower sealing contact surfaces after simulating the sealing performance using the structure in Figure 2c. The simulation results show that the maximum pressure on the upper sealing contact surface was 0.95 MPa, and the maximum pressure on the lower sealing contact surface was 0.48 MPa. The sealing gasket with this new structure also meets the requirement that the maximum pressure on the contact surface be greater than the gas pressure and the allowable stress.

For the sealing of gas–liquid inlets and outlets of the metal bipolar plate, in this paper, we further optimized the structure of the metal plate based on the double-peak sealing pad with the wings extension and arranged the sealing grooves of the anode plate and cathode plate in a staggered layout, as shown in Figure 2d. Figure 12 shows the pressure distribution on the sealing contact surfaces, which was simulated by using the offset sealing structure NO. 4 gasket in Figure 2d. It can be seen that the maximum contact pressure on the upper and lower contact surfaces was 1.2 MPa and 0.67 MPa, respectively, which is greater than the given gas pressure of 0.1 MPa. This indicates that the sealing structure of Figure 2d is reasonable for sealing the gas–liquid inlets and outlets of the metal bipolar plate.

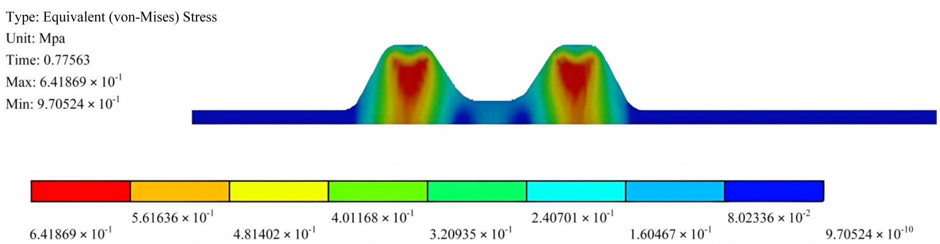

Figure 10. Equivalent stress distribution of the double-peak sealing gasket with extended wings.

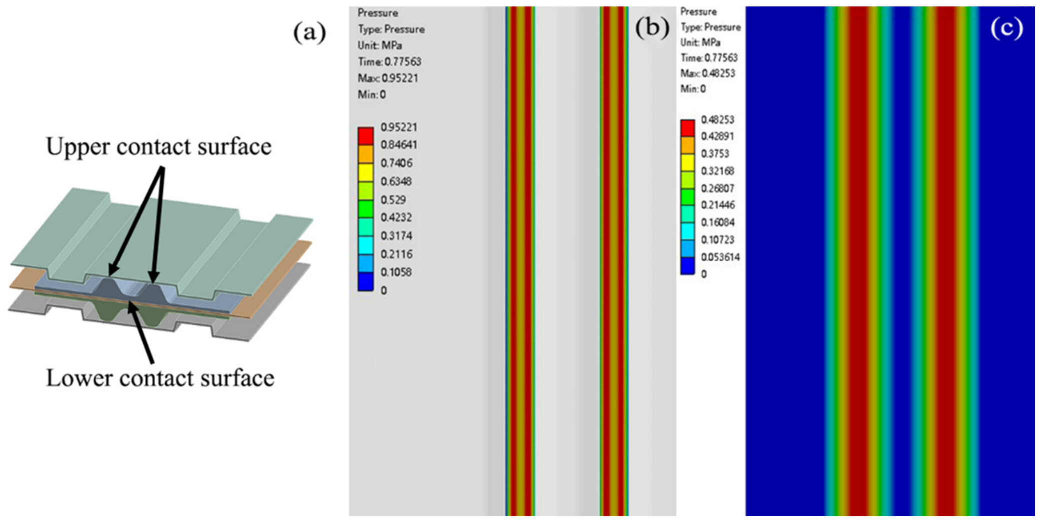

Figure 11. Pressure distribution on the contact surface of the seal structure NO. 3 gasket. (**a**) Sealing structure, (**b**) upper contact surface, (**c**) lower contact surface.

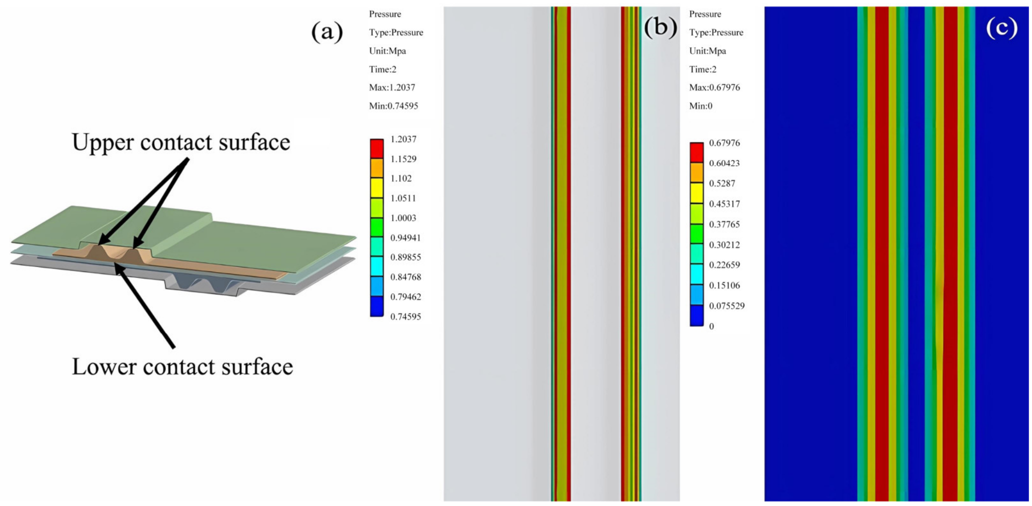

Figure 12. Pressure distribution on the contact surface of the offset sealing structure NO. 4 gasket. (**a**) Sealing structure, (**b**) upper contact surface, (**c**) lower contact surface.

In summary, combining the sealing structures NO. 3 and NO. 4 of Figure 2c,d, a complete set of metal bipolar plate-sealing gaskets can be designed for sealing performance testing analysis with membrane electrodes.

4.2. Comparison of Sealing Materials with Different Hardness

The material properties of sealing materials are one of the critical factors affecting sealing performance, and different hardnesses of the same type of rubber can also affect sealing performance. This article studies hardness's effect on EPDM rubber's sealing performance with hardnesses of 45 Shore A, 50 Shore A, 55 Shore A, and 60 Shore A. The simulation model adopted the sealing structure of the double-peak seal gasket with two-wing extension shown in Figure 2c, where the friction coefficient was set to 0.05 and the compression ratio was controlled at 35%. Figure 13 shows the relationship between contact pressure and rubber hardness, where Figure 13a shows the maximum contact pressure distribution corresponding to different hardness rubbers. Figure 13b shows the fitting curve of rubber hardness and the maximum contact pressure. The data in Figure 13a show that these four hardness rubbers meet the sealing requirements of Equation (4) under a friction coefficient of 0.05 and a compression ratio of 35%. According to the fitting equation of the data in Figure 13b, the fitting equations for the maximum contact pressure on the upper and lower contact surfaces are shown in Equations (8) and (9), respectively. This indicates that the contact pressure and rubber hardness have an exponential relationship, and an increase in rubber hardness will sharply increase the contact pressure on the contact surface, causing significant deformation of the metal bipolar plate. Therefore, to avoid damage to the metal bipolar plate caused by deformation, rubber with a hardness of 45 Shore A can be selected for subsequent testing and analysis verification.

$$\sigma_1 = 0.054489 + 0.10408e^{(0.05682H)} \tag{8}$$

$$\sigma_2 = 0.81988 + 0.0003096e^{(0.13565H)} \tag{9}$$

where σ_1 represents the upper contact surface pressure, σ_2 represents the lower contact surface pressure, and H represents the rubber hardness.

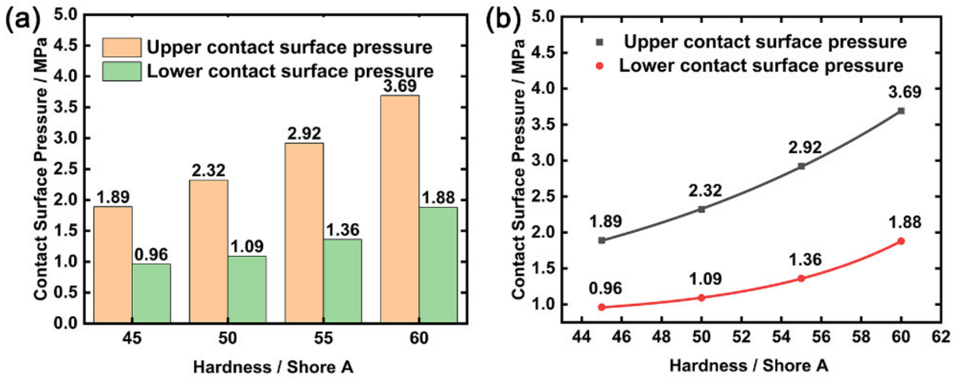

Figure 13. Relationship between the upper and lower contact surface pressure and hardness. (**a**) Pressure distribution diagram, (**b**) fitted curve.

4.3. Comparison of Different Coefficients of Friction

During the stack assembly process of the metal bipolar plate and rubber seal in the fuel cell, the contact surface under the stacking pressure will experience relative sliding friction, generating wear and heat and leading to the seal's failure. To investigate the effect of the friction coefficient of the contact surface on the sealing performance, the simulation model still uses the double-peak seal structure with wings extended outside the two sides in Figure 2c. The hardness of the sealing material is selected as 45 Shore A, and the compression ratio is controlled at 35%. Four different friction coefficients of 0.05, 0.1, 0.15, and 0.2 are simulated. Figure 14 shows the relationship between the contact surface pressure and the friction coefficient. Figure 14a shows the pressure distribution results of the upper and lower contact surfaces, while Figure 14b shows the maximum contact pressure curve of the upper and lower contact surfaces. Because metal bipolar plates adopt stamping forming technology, their surface roughness usually reaches over 10um, while for rubber materials, it is easy to achieve high flatness and smoothness, and there may be interface leakage between the bipolar plate and the gasket. Figure 13 shows that the contact pressure increases with the increase in the friction coefficient. Studies have shown that sufficient contact pressure is crucial for the sealing performance. By increasing the contact pressure, a lower leakage rate can be achieved [36]. In addition, the friction coefficient is related to roughness and increases with the increase in roughness [37]. Thus, for a sealing structure composed of a sealing gasket and metal bipolar plates, high roughness means high contact pressure. On the basis of meeting the sealing performance, materials with lower roughness can be selected to reduce the pressure inside the stack. Figure 14a indicates that these four friction coefficients satisfy the sealing requirements of Equation (4) at a compression ratio of 35% and a rubber hardness of 45 Shore A. Considering the condition of water lubrication, a friction coefficient of 0.05 can be used.

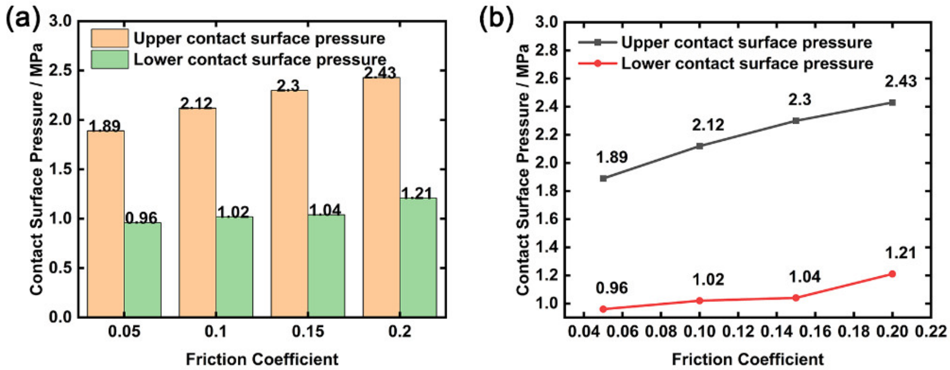

Figure 14. Relationship between the upper and lower contact surface pressure and friction coefficient. (**a**) Pressure distribution diagram. (**b**) Line chart.

4.4. Comparison of Different Compression Ratios

Compression ratio refers to the compression deformation ratio of the cross-section of the rubber seal when it is loaded into the sealing groove and compressed. The compression ratio of the rubber seal is directly related to the sealing performance of the metal bipolar plate. If the compression ratio is too low, it will directly lead to leakage of the sealing surface, and if the compression ratio is too large, it will easily cause the seal to fail and deform the metal plate. This paper selected rubber compression ratios of 25%, 30%, 35%, and 40% for simulation and analysis of their effects on the sealing performance of the metal bipolar plate. The simulation model still uses the double-peak seal structure with two wings extended outside the sealing pad, as shown in Figure 2c, with a seal material hardness of 45 Shore A and a friction coefficient of 0.05. Figure 15 shows the relationship between the contact surface pressure and the compression ratio; Figure 15a shows the pressure distribution of the upper and lower contact surfaces; and Figure 15b shows the fitting curve of the maximum contact pressure simulation results. Figure 15a shows that all four compression ratios meet the sealing requirements of Equation (4). Since the MEA requires a compression ratio of 20% to 30%, when the sealing pad has a compression ratio of 35%, the membrane electrode can reach an approximate compression ratio of 25%. Based on the fitting curves in Figure 15b, the fitting equations for the upper and lower contact surface pressures are given by Equations (10) and (11), respectively. This shows that the contact surface pressure and the rubber compression ratio approximately exhibit an exponential relationship. As the compression ratio increases, the contact pressure gradually increases. This way, the contact pressure is higher and the sealing gasket has better self-sealing performance [36]. The contact area also increases with the increase in compression ratio, that is, the larger the compression ratio, the longer the sealing path, which can enhance the sealing performance. However, the exponential increase in stress increases the risk of material failure. Thus, when designing PEMFC, it is necessary to choose an appropriate compression ratio to achieve self-sealing and reduce sealing failure.

$$\sigma_1 = 0.21267 + 0.10683e^{(0.07762\delta)} \tag{10}$$

$$\sigma_2 = -0.93235 + 0.7764e^{(0.02501\delta)} \tag{11}$$

where σ_1 represents the pressure on the upper contact surface, σ_2 represents the pressure on the lower contact surface, and δ represents the compression ratio of the rubber.

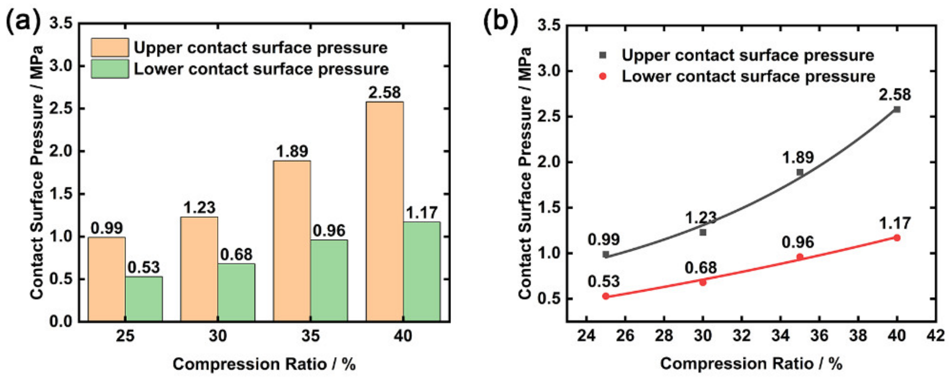

Figure 15. Relationship between the upper and lower contact surface pressure and compression ratio. (**a**) Pressure distribution diagram. (**b**) Fitted curve.

4.5. Experimental Analysis and Verification of Sealing Structure

According to the sealing test process, a metal bipolar plate seal made of the two-wing extended bimodal sealing structure shown in Figure 2c,d was assembled into a single fuel cell for sealing tests. Table 3 shows the leakage data of the tested single fuel cell at different compression ratios. At compression ratios of 25% and 30%, with pressure differences of 25 kPa and 6 kPa, respectively, which are far more significant than the sealing requirements of pressure drops within 3 kPa, the gas was not tightly sealed and the sealing performance was unqualified. After the compression ratio of the sealing gasket reached 35%, the sealing performance met the requirements.

Table 3. Leakage data of the tested single fuel cell at different compression ratios.

Compression Ratio δ/%	Initial Pressure/kPa	End Pressure/kPa	Pressure Difference/kPa
25	100	75	25
30	100	94	6
35	100	99	1
40	100	99	1

Using the simulation data of the contact pressure and compression ratio from Figure 15, the sealing performance was calculated, and the results are shown in Table 3. Combined with Equation (7), it can be seen from Table 4 that when the compression ratio was 25% and 30%, the equation was not satisfied, indicating that the sealing performance did not meet the standard. The equation was fully satisfied when the compression ratio exceeded 35%, indicating that the sealing requirements were met. This is consistent with the experimental results in Table 3, which verifies the accuracy of the simulation model.

Table 4. Sealing performance calculation at different compression ratios.

Compression Ratio δ/%	$\mu \cdot \bar{\sigma} \cdot L$/(MPa·mm)		$P \cdot h$/ (MPa·mm)
	Upper Contact Surface	Lower Contact Surface	
25	0.042	0.039	0.064
30	0.062	0.049	0.059
35	0.084	0.061	0.055
40	0.107	0.072	0.051

5. Conclusions

In this paper, the metal rubber composite sealing structure in the fuel cell metal stack was studied. An innovative double-peak sealing gasket structure was adopted to solve the problems of sealing leakage and deformation in PEMFCs. Based on the Mooney–Rivlin constitutive model, the influence of sealing material hardness, friction coefficient, and compression ratio on the sealing performance of the metal bipolar plate was explored and analyzed. The results are as follows:

1. A double-peak sealing gasket structure with two extended wings had a better sealing effect when it was in contact with the membrane electrode frame. In addition, a new type of offset sealing structure optimization was able to effectively improve the sealing effect at the gas–liquid inlet and outlet of the metal bipolar plate.
2. The maximum contact pressure values on the upper and lower contact surfaces were 1.89 MPa and 0.96 MPa, respectively, for EPDM rubber with a hardness of 45 Shore A, and 3.69 MPa and 1.88 MPa, respectively, for EPDM rubber with a hardness of 60 Shore A. And the contact pressure between the metal rubber seal and the plate increased exponentially with the hardness of the rubber, causing significant deformation of the metal bipolar plate.
3. The larger the friction coefficient of the metal rubber, the greater the contact pressure at the sealing contact surface, but the change in pressure is relatively smooth. Considering the condition of water lubrication, a friction coefficient of 0.05 could be recommended for adoption.
4. The maximum contact pressure on the upper contact surfaces increased from 1.89 MPa to 2.58 MPa, while the compression ratio increased from 35% to 40%. The contact pressure between the metal rubber seal and the plate was approximately exponential with the compression ratio of the rubber, and the contact pressure gradually increased with the increase in the compression ratio. Therefore, it is necessary to limit the compression ratio of the sealing gasket according to the requirements of the MEA in practical engineering.
5. The double-peak sealing gasket with extended wings was fabricated and assembled into a single fuel cell for testing. The results showed that the simulation and experimental sealing performance of the sealing gasket under different compression ratios remained similar. In order to ensure the sealing effect of the fuel cell metal stack, the sealing structure parameters can be referred to as follows: the roughness of the bipolar plate should be controlled within 0.08 mm; the hardness of the EPDM rubber should be 45 Shore A; the friction coefficient should be 0.05; and the initial compression ratio should be 35%. The results of this study can provide a reference for the sealing structure design of large metal bipolar plates in PEMFCs.

Author Contributions: Conceptualization, J.Z.; Methodology, J.Z., H.G. and Z.W.; Software, Z.G.; Formal analysis, H.G.; Investigation, S.P. and Z.G.; Resources, W.L.; Data curation, W.L. and Y.Y.; Writing—original draft, J.Z.; Writing—review & editing, S.P., Z.W. and T.M.; Visualization, Y.Y. and W.S.; Supervision, T.M.; Project administration, W.S. All authors have read and agreed to the published version of the manuscript.

Funding: This research received no external funding.

Institutional Review Board Statement: Not applicable.

Informed Consent Statement: Not applicable.

Data Availability Statement: Not applicable.

Conflicts of Interest: The authors declare no conflict of interest.

References

1. Daud, W.; Rosli, R.; Majlan, E.; Hamid, S.; Mohamed, R.; Husaini, T. PEM fuel cell system control: A review. *Renew. Energy* **2017**, *113*, 620–638. [CrossRef]
2. Corigliano, O.; Pagnotta, L.; Fragiacomo, P. On the Technology of Solid Oxide Fuel Cell (SOFC) Energy Systems for Stationary Power Generation: A Review. *Sustainability* **2022**, *14*, 15276. [CrossRef]
3. Fragiacomo, P.; Genovese, M.; Piraino, F.; Corigliano, O.; De Lorenzo, G. Hydrogen-Fuel Cell Hybrid Powertrain: Conceptual Layouts and Current Applications. *Machines* **2022**, *10*, 1121. [CrossRef]

4. Fragiacomo, P.; Piraino, F.; Genovese, M.; Corigliano, O.; De Lorenzo, G. Strategic Overview on Fuel Cell-Based Systems for Mobility and Electro-lytic Cells for Hydrogen Production. *Procedia Comput Sci.* **2022**, *200*, 1254–1263. [CrossRef]
5. Miyake, J.; Ogawa, Y.; Tanaka, T.; Ahn, J.; Oka, K.; Oyaizu, K.; Miyatake, K. Rechargeable proton exchange membrane fuel cell containing an intrinsic hydro-gen storage polymer. *Commun. Chem.* **2020**, *3*, 138. [CrossRef]
6. Lim, B.; Majlan, E.; Daud, W.; Rosli, M.; Husaini, T. Three-dimensional study of stack on the performance of the proton exchange membrane fuel cell. *Energy* **2019**, *169*, 338–343. [CrossRef]
7. Shi, D.; Cai, L.; Zhang, C.; Chen, D.; Pan, Z.; Kang, Z.; Zhang, J. Fabrication methods, structure design and durability analysis of advanced sealing ma-terials in proton exchange membrane fuel cells. *Chem. Eng. J.* **2022**, *454*, 139995. [CrossRef]
8. Pehlivan-Davis, S.; Clarke, J.; Armour, S. Comparison of accelerated aging of silicone rubber gasket material with aging in a fuel cell environment. *J. Appl. Polym. Sci.* **2013**, *129*, 1446–1454. [CrossRef]
9. Bhargava, S.; O'Leary, K.A.; Jackson, T.C.; Lakshmanan, B. Durability testing of silicone materials for proton exchange membrane fuel cell use. *Rubber Chem. Technol.* **2013**, *86*, 28–37. [CrossRef]
10. De Bruijn, F.A.; Dam, V.A.T.; Janssen, G.J.M. Review: Durability and Degradation Issues of PEM Fuel Cell Components. *Fuel Cells* **2008**, *8*, 3–22. [CrossRef]
11. Liang, P.; Qiu, D.; Peng, L.; Yi, P.; Lai, X.; Ni, J. Structure failure of the sealing in the assembly process for proton exchange membrane fuel cells. *Int. J. Hydrog. Energy* **2017**, *42*, 10217–10227. [CrossRef]
12. Wang, Z.; Tan, J.; Wang, Y.; Liu, Z.; Feng, Q. Chemical and mechanical degradation of silicone rubber under two compression loads in simulated proton-exchange membrane fuel-cell environments. *J. Appl. Polym. Sci.* **2019**, *136*, 47855. [CrossRef]
13. Tan, J.; Chao, Y.; Yang, M.; Lee, W.-K.; Van Zee, J. Chemical and mechanical stability of a Silicone gasket material exposed to PEM fuel cell environment. *Int. J. Hydrog. Energy* **2011**, *36*, 1846–1852. [CrossRef]
14. Tan, J.; Chao, Y.; Van Zee, J.; Li, X.; Wang, X.; Yang, M. Assessment of mechanical properties of fluoroelastomer and EPDM in a simulated PEM fuel cell environment by microindentation test. *Mater. Sci. Eng. A* **2008**, *496*, 464–470. [CrossRef]
15. Tan, J.; Chao, Y.; Van Zee, J.; Lee, W. Degradation of elastomeric gasket materials in PEM fuel cells. *Mater. Sci. Eng. A* **2007**, *445–446*, 669–675. [CrossRef]
16. Schulze, M.; Knöri, T.; Schneider, A.; Gülzow, E. Degradation of sealings for PEFC test cells during fuel cell operation. *J. Power Sources* **2004**, *127*, 222–229. [CrossRef]
17. Lin, C.W.; Chien, C.H.; Tan, J.; Chao, Y.J.; Van Zee, J.W. Chemical degradation of five elastomeric seal materials in a simulated and an accelerated PEM fuel cell environment. *J. Power Sources* **2011**, *196*, 1955–1966. [CrossRef]
18. Mitra, S.; Ghanbari-Siahkali, A.; Kingshott, P.; Rehmeier, H.K.; Abildgaard, H.; Almdal, K. Chemical degradation of crosslinked ethylene-propylene-diene rub-ber in an acidic environment. Part I. Effect on accelerated sulphur crosslinks. *Polym. Degrad. Stab.* **2006**, *91*, 69–80. [CrossRef]
19. Mitra, S.; Ghanbari-Siahkali, A.; Kingshott, P.; Almdal, K.; Rehmeier, H.K.; Christensen, A.G. Chemical degradation of fluoroelastomer in an alkaline environment. *Polym. Degrad. Stab.* **2004**, *83*, 195–206. [CrossRef]
20. Feng, J.; Zhang, Q.; Tu, Z.; Tu, W.; Wan, Z.; Pan, M.; Zhang, H. Degradation of silicone rubbers with different hardness in various aqueous solutions. *Polym. Degrad. Stab.* **2014**, *109*, 122–128. [CrossRef]
21. Cui, T.; Chao, Y.; Van Zee, J. Sealing force prediction of elastomeric seal material for PEM fuel cell under temperature cycling. *Int. J. Hydrog. Energy* **2014**, *39*, 1430–1438. [CrossRef]
22. Cui, T.; Chao, Y.; Van Zee, J. Thermal stress development of liquid silicone rubber seal under temperature cycling. *Polym. Test.* **2013**, *32*, 1202–1208. [CrossRef]
23. Chien, C.-H.; Lin, C.-W.; Chao, Y.-J.; Tong, C.; Van Zee, J. Compression of Seals in PEM Fuel Cells. *Exp. Mech. Emerg. Energy Sys. Mater.* **2011**, *5*, 183–192. [CrossRef]
24. Zhang, J.; Hu, Y. Sealing performance and mechanical behavior of PEMFCs sealing system based on thermodynamic coupling. *Int. J. Hydrog. Energy* **2020**, *45*, 23480–23489. [CrossRef]
25. Achenbach, M. Service life of seals—Numerical simulation in sealing technology enhances prognoses. *Comput. Mater. Sci.* **2000**, *19*, 213–222. [CrossRef]
26. Achenbach, M. Development of a robust fuel circuitsealing system: Achieving a solution. *Seal Technol.* **2007**, *2007*, 7–10. [CrossRef]
27. Su, Z.Y.; Liu, C.T.; Chang, H.P.; Li, C.H.; Huang, K.J.; Sui, P.C. A numerical investigation of the effects of compression force on PEM fuel cell performance. *J. Power Sources* **2008**, *183*, 182–192. [CrossRef]
28. Xing, S.; Zhao, C.; Liu, W.; Zou, J.; Chen, M.; Wang, H. Effects of bolt torque and gasket geometric parameters on open-cathode polymer electrolyte fuel cells. *Appl. Energy* **2021**, *303*, 117632. [CrossRef]
29. Huang, X.; Liu, S.; Yu, X.; Liu, Y.; Zhang, Y.; Xu, G. A mechanism leakage model of metal-bipolar-plate PEMFC seal structures with stress relaxation effects. *Int. J. Hydrog. Energy* **2022**, *47*, 2594–2607. [CrossRef]
30. Qiu, D.; Liang, P.; Peng, L.; Yi, P.; Lai, X.; Ni, J. Material behavior of rubber sealing for proton exchange membrane fuel cells. *Int. J. Hydrog. Energy* **2020**, *45*, 5465–5473. [CrossRef]
31. Cleghorn, S.; Mayfield, D.; Moore, D.; Moore, J.; Rusch, G.; Sherman, T.; Sisofo, N.; Beuscher, U. A polymer electrolyte fuel cell life test: 3 years of continuous operation. *J. Power Sources* **2006**, *158*, 446–454. [CrossRef]
32. Tan, J.; Chao, Y.J.; Li, X.; Van Zee, J.W. Degradation of silicone rubber under compression in a simulated PEM fuel cell environment. *J. Power Sources* **2007**, *172*, 782–789. [CrossRef]

33. Basuli, U.; Jose, J.; Lee, R.H.; Yoo, Y.H.; Jeong, K.-U.; Ahn, J.-H.; Nah, C. Properties and Degradation of the Gasket Component of a Proton Exchange Membrane Fuel Cell—A Review. *J. Nanosci. Nanotechnol.* **2012**, *12*, 7641–7657. [CrossRef]
34. Tan, J.; Chao, Y.; Wang, H.; Gong, J.; Van Zee, J. Chemical and mechanical stability of EPDM in a PEM fuel cell environment. *Polym. Degrad. Stab.* **2009**, *94*, 2072–2078. [CrossRef]
35. Cui, T.; Chao, Y.; Van Zee, J. Stress relaxation behavior of EPDM seals in polymer electrolyte membrane fuel cell environment. *Int. J. Hydrog. Energy* **2012**, *37*, 13478–13483. [CrossRef]
36. Xu, Q.; Zhao, J.; Chen, Y.; Liu, S.; Wang, Z. Effects of gas permeation on the sealing performance of PEMFC stacks. *Int. J. Hydrog. Energy* **2021**, *46*, 36424–36435. [CrossRef]
37. Palasantzas, G. Influence of self-affine roughness on the adhesive friction coefficient of a rubber body sliding on a solid substrate. *Surf. Sci.* **2004**, *565*, 191–196. [CrossRef]